Journal of the Korean Physical Society, Vol. 53, No. 5, November 2008, pp. 2811∼2815

Ab-Initio Studies of Electronic and Spectroscopic Properties of MgO, ZnO and CdO

A. Schleife,* C. Rödl, F. Fuchs, J. Furthmüller and F. Bechstedt
Institut für Festkörpertheorie und-optik, Friedrich-Schiller-Universität and European Theoretical Spectroscopy Facility (ETSF), Max-Wien-Platz 1, 07743 Jena, Germany

P. H. Jefferson, T. D. Veal and C. F. McConville
Department of Physics, University of Warwick, Coventry, CV4 7AL, U.K.

L. F. J. Piper, A. DeMasi and K. E. Smith
Department of Physics, Boston University, 590 Commonwealth Avenue, Boston, MA 02215, U.S.A.

H. Lösch and R. Goldhahn
Institut für Physik, Weimarer Straße 32, 98693 Ilmenau, Germany

C. Cobet
Institute for Analytical Sciences, Albert-Einstein-Straße 9, 12489 Berlin, Germany

J. Zúñiga-Pérez and V. Muñoz-Sanjosé
Depatamento de Física Aplicada y Electromagnetismo, Universitat de València, C/ Dr. Moliner 50, 46100 Burjassot, Spain

(Received 10 September 2007)

We present *ab-initio* calculations of excited-state properties within single-particle and two-particle approaches in comparison with corresponding experimental results. For the theoretical treatment of the electronic structure, we compute eigenvalues and eigenfunctions by using a spatially nonlocal exchange-correlation potential. From this starting point, quasiparticle energies within the fully frequency-dependent G_0W_0 approximation are obtained. By solving the Bethe-Salpeter equation, we evaluate optical properties, including the electron-hole attraction and the local-field effects. The results are compared with experimental spectra from soft X-ray emission, as well as from X-ray photoelectron spectroscopy or ellipsometry measurements. In more detail, we compute the valence-band densities of states, bound excitons, and the dielectric function. For the latter, we discuss both the absorption edge and higher critical points.

PACS numbers: 71.35.-y, 71.20.-b, 71.55.Gs
Keywords: Ab initio calculations, Density functional theory, II-VI semiconductors, Quasiparticles, Density of states, Excitons, X-ray emission, X-ray photoelectron spectroscopy, Dielectric function

I. INTRODUCTION

Being a possible candidate for applications in optoelectronic devices and being environmentally friendly, ZnO has strongly re-attracted interest in the last years. Other group-II metal oxides, like MgO and CdO, are discussed in the context of spintronics (together with transition-metal oxides), alloys, or heterostructures. ZnO [1] and MgO [2] allow for the formation of new types of nanostructures, such as nanorods, -rings, -brushes, and -tubes. From a theoretical point of view, comparably little is known about the influence of shallow d electrons on the electronic structures, *e.g.*, gaps and densities of states. Also, the optical properties of ZnO, especially excitonic effects, have not yet been studied over a wide spectral range. A better fundamental understanding of the electronic structure of all the three oxides would undoubtedly be helpful for interpreting experimental results.

Starting from a detailed investigation of the structural and electronic properties of these materials in the framework of density functional theory (DFT) using the Kohn-Sham (KS) approach [3], we present *ab-initio* calcula-

*E-mail: schleife@ifto.physik.uni-jena.de

tions of the band structures and the densities of states (DOS), including quasiparticle (QP) corrections.

II. METHODS

The computational part is carried out applying DFT as implemented in the Vienna *Ab initio* Simulation Package (VASP) [4] with the same computational parameters as described in Ref. 3 unless otherwise noted. The shallow Zn $3d$ and Cd $4d$ electrons are treated as valence electrons. Spin-orbit coupling (SOC) is included in the DFT calculations [5]. The experimental part includes soft X-ray emission (SXE) and high-resolution X-ray photoemission spectroscopy (XPS) measurements. SXE spectroscopy is a second-order optical process, where a core hole electron is excited above the absorption threshold. This excited state decays by a radiative transition of a valence electron into an empty core-hole. Along with being element-specific due to the core level, dipole selection rules ($\Delta l = \pm 1$) govern the transition, and SXE directly measures the orbital-angular-momentum-resolved partial density of states (PDOS) [6]. In the present work we have employed SXE of the O K edge to directly measure the occupied O $2p$ PDOS.

For the computation of the electronic structure, we solve the QP problem by using the GW approximation [7] of the self energy. However, for ZnO and CdO, the standard approach for the computation of QP energies, *i.e.*, the application of perturbation theory on top of a starting point from a generalized-gradient approximation (GGA) calculation [8, 9], is not successful. Therefore, we use the spatially nonlocal HSE03 [10] exchange-correlation (XC) functional in the context of a generalized KS scheme [11]. The Dyson equation itself is then expanded in terms of the generalized KS eigenvalues and eigenfunctions. The idea behind this procedure is that the standard one-shot perturbation-theory approach for the computation of QP energies is better justified when these nonlocal XC functionals are used to compute the starting electronic structure. It has been demonstrated that the resulting eigenvalues (and eigenfunctions) are closer to the *true* QP values than in the case of GGA [9]. The succeeding GW calculation incorporates the fully frequency-dependent dielectric function [12] and yields QP energies that are directly comparable to measurements. This procedure is computationally more demanding than a calculation using a local or semilocal XC functional; thus, we have to restrict the **k**-point meshes for the Brillouin zone (BZ) integrations to $8 \times 8 \times 6$ for ZnO and $10 \times 10 \times 10$ for MgO and CdO. Tests indicate that this yields results for the QP energies that are converged up to $10 - 20$ meV.

The experiments for MgO and CdO were performed at the soft X-ray undulator beamline X1B at the National Synchrotron Light Source (NSLS), Brookhaven National Laboratory, which is equipped with a spherical grating monochromator. The incident energy was set to 555 eV. The emitted X-ray photons were measured using a Nordgren-type grazing-incidence grating spectrometer set to energy resolutions of 0.55 eV (MgO) and 0.37 eV (CdO) at the O K-edge region [13]. The emission energy axis was calibrated to second order in the L edge of Zn. The XPS measurements for ZnO were taken within a conventional ultrahigh-vacuum chamber by using a Scienta ESCA300 spectrometer at the National Centre for Electron Spectroscopy and Surface analysis (NCESS), Daresbury Laboratory, UK. The Al K_α X-ray source ($h\nu = 1486.6$ eV) was monochromated, and the instrumental resolution was 0.45 eV. The Fermi level position (zero of the binding energy scale) was calibrated using the Fermi edge of a silver reference sample. In the calculations, we incorporated a Gaussian broadening of 0.45-eV FWHM for all the materials.

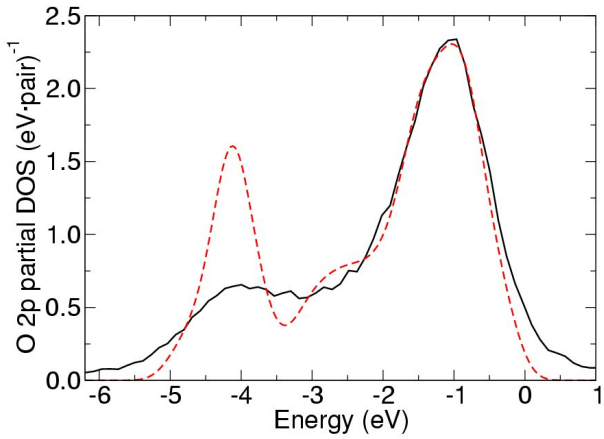

Fig. 1. O $2p$ PDOS of rs-MgO: The experimental curve (solid black) is obtained from SXE measurements from the O K edge. The theoretical (dashed red) curve is computed using the HSE03 functional and a succeeding GW calculation.

III. ELECTRONIC PROPERTIES

The calculated PDOS of the O $2p$ electrons for MgO in the rocksalt (rs) structure is plotted in Figure 1, together with the experimental SXE data. The O $2p$ states are located in the energy region between -6 and 0 eV, with pronounced peaks at -4.2 eV and -1.2 eV. The agreement between theory and experiment regarding the peak positions is quite good. However, for the relative peak heights or peak intensities, it is worse. In the calculations, we find an overestimate of the height of the peak lower in energy with respect to the other one. We observe this trend for each of the studied oxides, which may be related to transition matrix element effects present in the experiment but neglected in our calculations. For MgO, a fundamental gap of 7.47 eV is computed, which is slightly smaller than the experimental value of 7.8 eV

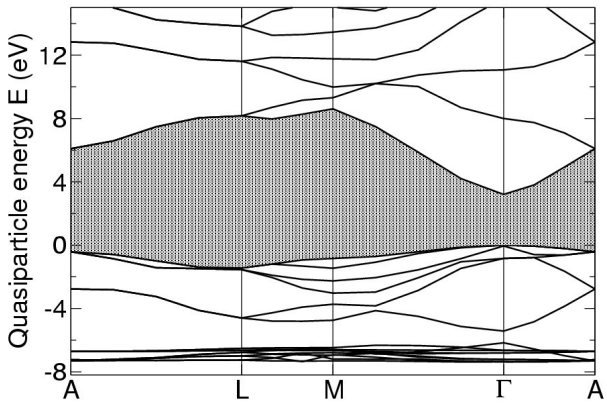

Fig. 2. Theoretical band structure of w-ZnO (without SOC) calculated using the HSE03 functional as starting point and corrected by using GW QP shifts. The VBM is used as energy zero.

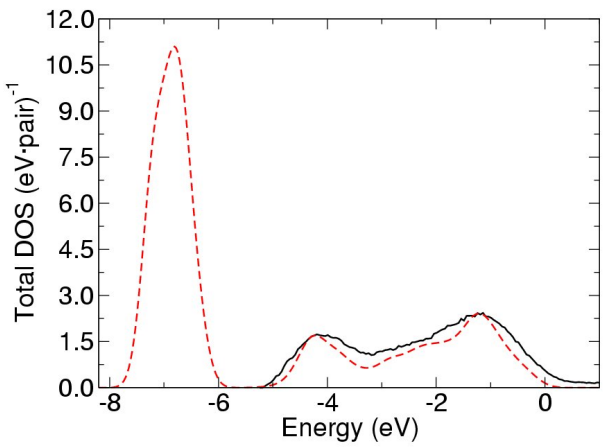

Fig. 3. Total DOS of w-ZnO: The experimental (solid black) curve is obtained from high-resolution XPS measurements. The theoretical (dashed red) curve is computed using the HSE03 functional and a succeeding GW calculation.

[14]. We find such an underestimate of the direct gap for all the oxides. One reason for this is that the HSE03 gaps are at least 1 eV smaller than the experimental values, and, therefore, still constitute a challenge to the one-step perturbation-theory approach applied in this work.

For ZnO in the wurtzite (w) structure, the computed QP band structure is plotted in Figure 2. In the band structure, the mean position of the Zn $3d$ bands at Γ is at about -6.96 eV. At higher energies, the O $2p$ states form the uppermost region of the valence bands. The calculated gap amounts to 3.2 eV, showing the previously discussed underestimate of the experimental gap of 3.4 eV [15]. In addition to the already mentioned reason, the presence of d electrons complicates the computational treatment of ZnO and CdO. Even the HSE03 functional underestimates the binding energy of the d electrons and, therefore, leads to an overestimate of the pd repulsion, with consequences as discussed in Ref. 16. The

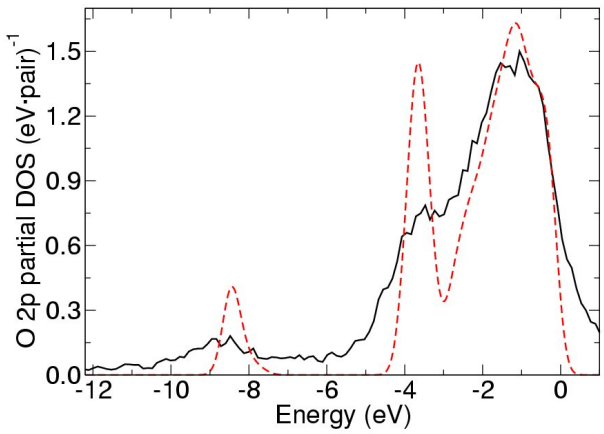

Fig. 4. O $2p$ PDOS of rs-CdO: The experimental curve (solid black) is obtained from SXE measurements from the O K edge. The theoretical (dashed red) curve is computed using the HSE03 functional and a succeeding GW calculation.

computed total DOS is plotted in Figure 3 in comparison with the curve from the XPS measurements. As in the case of MgO, Figure 3 shows two pronounced peaks caused by the O $2p$ states. For ZnO, we also find a very good agreement for the relative peak heights. The theoretical curve reveals a peak caused by Zn $3d$ states which is located around -6.96 eV, while the experimental value of about -6.95 eV [17] is somewhat lower. As already mentioned, this may be one of the reasons for the underestimate of the gaps in the calculations.

In Figure 4, the O $2p$ PDOS for rs-CdO is plotted, together with the experimental curve from the SXE measurements. In the energy region where the d states are located, we find an additional peak at about -8.4 eV because of the hybridization of the p and the d states. The experimental position of this peak is about 0.4 eV lower in energy than the theoretical one. The computed direct gap at Γ of 1.90 eV is smaller than the experimental value of 2.28 eV cited in Ref. 18. The agreement is better for the indirect gap between the valence band maximum (VBM) at the L point and the conduction band minimum (CBM) at Γ: we obtain a value of 0.81 eV while the experimental result amounts to 0.84 eV, as cited in Ref. 18.

IV. OPTICAL PROPERTIES

In the second part, we focus on the optical properties of ZnO. We compute the frequency-dependent dielectric function for the bulk crystal from first principles by solving the Bethe-Salpeter equation (BSE) and compare the results with those from spectral ellipsometry measurements. Furthermore, bound states below the QP gap are studied by applying this approach. To account for excitonic and local-field effects, we include the screened electron-hole attraction and a bare electron-hole

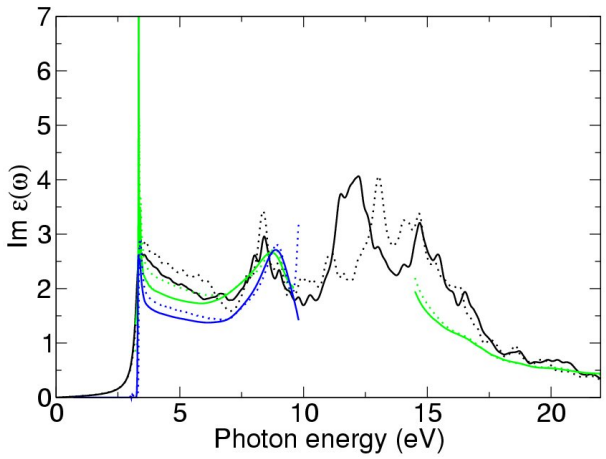

Fig. 5. Black curves: Computed imaginary part of the dielectric function of w-ZnO for ordinary (solid) and extraordinary (dotted) polarization. The experimental curves result from spectral ellipsometry measurements at 130 K (green curves) and at room temperature (red curves) and have partially been carried out at BESSY II.

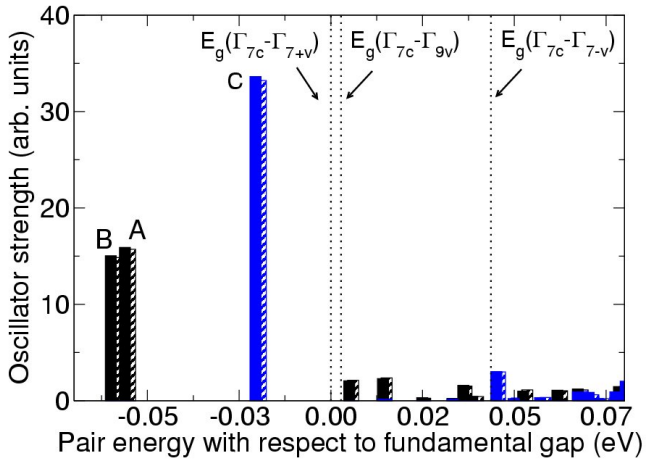

Fig. 6. Oscillator strengths vs. binding energy for the lowest electron-hole pair states. Black: $\mathbf{E} \perp \mathbf{c}$; blue: $\mathbf{E} \parallel \mathbf{c}$. The different shadings represent the different orientations of the total angular momentum. The lowest QP gap between Γ_{7c} and Γ_{7+v} is used as energy zero.

exchange term [19,20]. The electron-hole pair Hamiltonian that includes all relevant Coulomb interaction matrix elements [16] is constructed, a task which is computationally very demanding with respect to memory and computation time. Therefore, we have to keep the number of involved electron-hole pairs as small as possible. For the bound excitons, the **k**-points around the direct gap at Γ are of special interest. For this reason, we use **k**-point meshes with an increased density in the region around Γ. This approach strongly reduces the numerical effort and allows us finally to carry out calculations with high accuracy; otherwise the involved matrices would exceed today's computational capabilities. The details of the BSE calculations using such *hybrid* **k**-point meshes will be described elsewhere [21]. In the end, we sample the outer region of the BZ by using a 8 × 8 × 6 MP mesh. In the inner region, covering 3/8 × 3/8 × 1/2 of the BZ, we refine the sampling by using 14 × 14 × 14 **k**-points. Altogether, this approach yields a number of 3064 **k**-points. SOC is taken into account via a perturbative approach: The differences between the KS eigenvalues from calculations with and without SOC are added to the QP energies that are used to construct the excitonic pair Hamiltonian.

The computation of a converged dielectric function necessitates a large number of pair states. For the low-energy region of the absorption spectrum up to ≈7 eV, quite a large number of **k**-points is necessary while for higher energies, it is more important to include a large number of bands. Therefore, the low-energy part of the dielectric function is evaluated using a hybrid mesh: the coarse mesh is again a 8 × 8 × 6 MP mesh while the inner 5/8 × 5/8 × 5/6-part of the BZ is filled with 14 × 14 × 14 **k**-points. For the high-energy part, using only the coarse mesh is sufficient.

Because of the large number of included states, it is practically impossible to compute the necessary single-particle wave functions and eigenvalues from a nonlocal XC functional. Instead of doing so, we apply the GGA+U method to generate eigenvalues and eigenfunctions [19]. We choose $U = 6.5$ eV so that the final QP band structure coincides as much as possible with the one we obtain for G_0W_0 on top of a DFT ground state computed with the HSE03 functional. For the computation of the dielectric function, QP energies are also necessary. For the low-energy part, a scissors shift of 1.97 eV is used to bring the GGA+U gap to the experimental value of 3.4 eV. For the high-energy region, we carry out a GW calculation in which the screened Coulomb interaction is computed using a model dielectric function [22].

We compute the *converged* ordinary and extraordinary imaginary parts of the dielectric function of w-ZnO (see Figure 5), including the electron-hole interaction. Beside the band-gap region, which is discussed below, the excitonic effects have a strong influence on the peak positions and the oscillator strengths in the range of the high-energy critical points above 7 eV, as compared with previous calculations without electron-hole interaction [3]. The polarization anisotropy is in good agreement with the experimental data, although the calculation slightly underestimates the position of the peak at about 8 eV, a problem that can be related to the underlying QP energies. The occurrence of this peak emerges from a high combined DOS of the O $2p$ valence and the upper conduction bands. The computed anisotropy above 15 eV is weak, which is again confirmed by using ellipsometry studies.

The polarization anisotropy for the bound excitonic states below the gap is of fundamental interest. In Figure 6, the oscillator strengths of each electron-hole pair

are plotted as a function of the corresponding pair energy near the band edge. The lowest bound-exciton state (B, $\Gamma_{7+v} \rightarrow \Gamma_{7c}$) at -59 meV exhibits a strong oscillator strength for $\mathbf{E} \perp \mathbf{c}$ and small values for $\mathbf{E} \parallel \mathbf{c}$. This is in agreement with the Γ_{7+v} character we find for the involved uppermost valence band states. The second bound-exciton state (A, $\Gamma_{9v} \rightarrow \Gamma_{7c}$) is roughly 4 meV higher in energy while the difference between A and C ($\Gamma_{7-v} \rightarrow \Gamma_{7c}$) is approximately 36 meV. These values are in excellent agreement with published measured splittings [23] of 5 meV and 40 meV, respectively, and with the theoretical results of Ref. 24. The excitonic bound states are Wannier-Mott-like, despite the partly non-parabolic character of the involved bands close to Γ.

ACKNOWLEDGMENTS

Use of the National Synchrotron Light Source, Brookhaven National Laboratory, is acknowledged. Parts of this work were supported by the U.S. Department of Energy, Office of Science, Office of Basic Energy Sciences under Contract No. DE-AC02-98CH10886. We also thank the Deutsche Forschungsgemeinschaft (Grant No. SCHL 1862/1-1 and Project No. Be 1346/18-2), the Thüringer Graduiertenförderung, and the EU Network of Excellence NANOQUANTA (Grant No. NMP4-CT-2004-500198) for financial support and the LRZ München for computing time. The ellipsometric studies at BESSY were supported by the BMBF (Grants Nos. 05KS4KTB/3 and 05ES3XBA/5). The Engineering and Physical Science Research Council is thanked for financial support under grant no. EP/E010210/1 and for access to the National Centre for Electron Spectroscopy and Surface analysis under grant no. GR/S14252/0.

REFERENCES

[1] C. Klingshirn, M. Grundmann, A. Hoffmann, B. Meyer and A. Waag, Physik J. **5**, 33 (2006).
[2] Y. B. Li, Y. Bando, D. Golberg and Z. W. Liu, Appl. Phys. Lett. **83**, 999 (2003).
[3] A. Schleife, F. Fuchs, J. Furthmüller and F. Bechstedt, Phys. Rev. B **73**, 245212 (2006).
[4] G. Kresse and J. Furthmüller, Phys. Rev. B **54**, 11169 (1996).
[5] D. Hobbs, G. Kresse and J. Hafner, Phys. Rev. B **62**, 11556 (2000).
[6] A. Kotani and S. Shin, Rev. Mod. Phys. **73**, 203 (2001).
[7] W. G. Aulbur, L. Jönsson and J. W. Wilkins, *Solid State Physics: Advances in Research and Applications* (Academic, San Diego, 2000), Vol. 54, p. 1.
[8] P. Rinke, A. Qteish, J. Neugebauer, C. Freysoldt and M. Scheffler, New J. Phys. **7**, 126 (2005).
[9] F. Fuchs, J. Furthmüller, F. Bechstedt, M. Shishkin and G. Kresse, Phys. Rev. B **76**, 115109 (2007).
[10] J. Heyd, G. E. Scuseria and M. Ernzerhof, J. Chem. Phys. **118**, 8207 (2003).
[11] A. Seidl, A. Görling, P. Vogl, J. A. Majewski and M. Levy, Phys. Rev. B **53**, 3764 (1996).
[12] M. Shishkin and G. Kresse, Phys. Rev. B **74**, 035101 (2006).
[13] J. Nordgren and R. Nyholm, Nucl. Instr. Meth. A **246**, 242 (1986).
[14] D. M. Roessler and W. C. Walker, Phys. Rev. **159**, 733 (1967).
[15] Y. S. Park, C. W. Litton, T. C. Collins and D. C. Reynolds, Phys. Rev. **143**, 512 (1966).
[16] J. Furthmüller, P. H. Hahn, F. Fuchs and F. Bechstedt, Phys. Rev. B **72**, 205106 (2005).
[17] R. T. Girard, O. Tjernberg, G. Chiaia, S. Söderholm, U. O. Karlsson, C. Wigren, H. Nylén and I. Lindau, Surf. Sci. **373**, 409 (1997).
[18] Y. Dou, R. G. Egdell, D. S. L. Law, N. M. Harrison and B. G. Searle, J. Phys. Cond. Mat. **10**, 8447 (1998).
[19] R. Laskowski and N. E. Christensen, Phys. Rev. B **73**, 045201 (2006).
[20] W. G. Schmidt, S. Glutsch, P. H. Hahn and F. Bechstedt, Phys. Rev. B **67**, 085307 (2003).
[21] F. Fuchs, C. Rödl, A. Schleife and F. Bechstedt, Phys. Rev B **78**, 085103 (2008).
[22] F. Bechstedt, R. Del Sole, G. Cappellini and L. Reining, Solid State Commun. **84**, 765 (1992).
[23] S. Tsoi, X. Lu, A. K. Ramdas, H. Alawadhi, M. Grimsditch, M. Cardona and R. Lauck, Phys. Rev. B **74**, 165203 (2006).
[24] W. R. Lambrecht, A. V. Rodina, S. Limpijumnong, B. Segall and B. Meyer, Phys. Rev. B **65**, 075207 (2002).